Travelling waves in a spring-block chain sliding down a slope

José Eduardo Morales Morales, Guillaume James, Arnaud Tonnelier

HAL Id: hal-01411516
https://inria.hal.science/hal-01411516

Submitted on 7 Dec 2016

Travelling waves in a spring-block chain sliding down a slope

J. E. M. Morales, G. James, A. Tonnelier

Travelling waves in a spring-block chain sliding down a slope

J. E. M. Morales, G. James, A. Tonnelier

Project-Team BIPOP

Research Report n° 8995 — December 2016 — 19 pages

Abstract: Travelling waves in a spring-block chain sliding down an inclined plane are studied. For a piecewise-linear spinodal friction force, we construct analytically front waves. Pulse waves are obtained as the matching of two travelling fronts with identical speeds. Explicit formulas are obtained for the wavespeed and the wave form in the anti-continuum limit. The link with propagating phenomena in the Burridge-Knopoff model is briefly discussed.

Key-words: Travelling front, block-spring system, excitability, piecewise-linear differential equations

Propagation d'ondes dans une chaîne de blocs glissant le long d'une pente.

Résumé : On étudie la propagation d'ondes dans une chaîne de bloc-ressort glissant sur un plan incliné. Pour une force de frottement *spinodale* linéaire par morceaux, nous construisons analytiquement des ondes de type *front*. Les ondes *pulses* sont obtenues comme la concaténation de deux fronts dont les vitesses de déplacement sont identiques. Des expressions explicites pour la forme de l'onde et sa vitesse sont obtenues dans la limite anti-continue. Le lien avec la propagation d'ondes dans le modèle de Burridge-Knopoff est brièvement discuté.

Mots-clés : Propagation d'ondes, système bloc-ressort, excitabilité, équation différentielle linéaire par morceaux

1   Introduction

Spatially discrete extended systems have a wide range of applications ranging from natural sciences to engineering or social sciences. In physics, they frequently appear as ideal mass spring systems with nearest-neighbours coupling and have been used extensively to describe the dynamics of microscopic structures such as the vibration in crystals or micromechanical arrays [12, 13, 18] or to approximate the macroscopic behaviour of deformable systems. Recent studies on soft media have driving a renewed interest in the dynamics of elastically coupled systems with a special emphasis on transition waves [17].

In this work we consider a spring-block system that slides down a slope due to gravity (see Fig. 1). Each block is subjected to a nonlinear friction force. This system offers a simple macroscopic model for the frictional interaction of two structures. We consider here a friction force of spinodal type (see Fig. 2 for an example). Such friction laws have been reported to induce excitable dynamics [3] reminiscent of neural excitability [11, 9], i.e., a perturbation above a certain threshold produces a large excursion in the phase space before returning to an equilibrium state. In biology, it is well documented that a large class of excitable media is able to support nonlinear solitary waves [15]. It has been recently shown that excitable mechanical systems also have the capacity to induce self-sustained solitary waves [6, 5, 14]. In contrast with classical excitable media, these systems are elastic rather than diffusive.

In many studies, the analysis of discrete travelling patterns heavily relies on a continuum approximation of the original model. In the spring-block model presented here, we directly tackle the discrete nature of the equations and use an idealized piecewise-linear friction force to derive exact expressions for propagating waves. This *bilinearization* approach has been used in a variety of contexts to study travelling waves in lattices, see e.g. [10, 3, 21, 8, 1, 23, 25, 24, 19, 20].

The paper is organized as follows. We first derive in Sec. 2 the governing equations for the chain of elastically coupled blocks. Then we study in Sec. 3 the dynamical properties of an isolated block and demonstrate that a bistable behaviour exists when a spinodal friction force is considered. In Sec. 4 we perform numerical simulations of the coupled system and show that the bistability property induces travelling patterns, such as fronts and pulses. In Sec. 5 we construct the travelling fronts analytically using a piecewise-linear friction force. The anti-continuum limit is studied in Sec. 6. The link between front and pulse waves is studied in Sec. 7. We then conclude by connecting the results to a dynamical model of an earthquake fault, the so-called Burridge-Knopoff stick-slip model.

2   Model

Let us consider an isolated block of mass m and position $x(t)$ that slips down a slope under gravity and subject to a velocity-dependent friction force $F\left(\frac{dx}{dt}\right)$. The dynamical equations read

$$m\frac{d^2x}{dt^2} + F\left(\frac{dx}{dt}\right) = G \tag{1}$$

where G is the tangential component of the gravity force. A steady state of (1) exists when the block achieves a constant velocity motion $\frac{dx}{dt} = V$ where $F(V) = G$. Let us consider an infinite chain of identical blocks linearly coupled through Hookean springs of stiffness k that slips at the constant speed V over an inclined surface (see Fig. 1). The dynamical equations in a frame

moving at velocity V are given by:

$$\frac{dy_n}{dt} = u_n,$$

$$m\frac{du_n}{dt} = k\Delta_d y_n - F(V + u_n) + G, \qquad n \in \mathbb{Z} \tag{2}$$

where y_n represents the displacement of the nth block from the steady sliding state and u_n its velocity. The term $\Delta_d y_n = y_{n+1} - 2y_n + y_{n-1}$ is the discrete Laplacian.
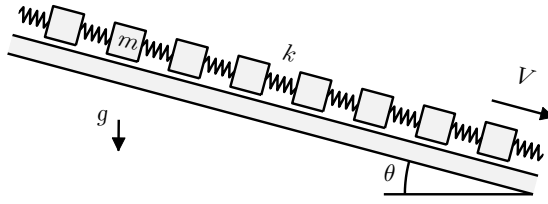
Figure 1: Mechanical representation of the block-spring slider model where m is the mass, k is the spring constant and V is the sliding velocity. The steady state corresponds to $F(V) = G$ with $G = mg\sin\theta$.

The system may be interpreted as a variant of the Burridge-Knopoff model [2] where the shear stress described by the local potential is replaced by a constant tangential force induced by gravity. The dynamics of system (2) is explored for three normalized non-monotonic friction laws F_ε, F_c and F_0, depicted in Fig. **2A-C** and given by

$$\begin{aligned}
F_\varepsilon(v) &= \left[1 - \alpha + \sqrt{N(v)}\right]\frac{v}{\sqrt{\varepsilon + v^2}}, \\
F_c(v) &= 3.2v^3 - 7.2v^2 + 4.8v, \\
F_0(v) &= v/a - \alpha H(v - a),
\end{aligned} \tag{3}$$

where $N(v) = \varepsilon + 4\max(|v| - a, 0)^2 + \alpha^2\max(a - |v|, 0)^2$, and H is the Heaviside step function. For convenience, the cubic friction force F_c is given for $a = 1$ where a is the location of the local minimum, i.e. the transition point from velocity-weakening ($v < a$) to velocity-strenghtening ($v > a$) regime. The friction function F_ε describes a regularized generalized Coulomb law as $\varepsilon \to 0$. The cubic friction force F_c describes a smooth spinodal friction law similar to the one introduced in [6]. The piecewise linear function F_0 reduces the velocity-weakening region to a jump discontinuity. It captures some properties of spinodal friction laws and is convenient for analytical computations.

3 Bistable single block dynamics

For a single block, (2) reads

$$\frac{dy}{dt} = u.$$

$$m\frac{du}{dt} = -F(V + u) + F(V). \tag{4}$$
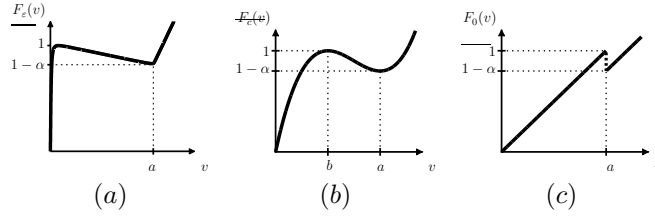
Figure 2: Non-monotonic friction laws. (a) Coulomb-like friction force F_ε, where $\varepsilon = 10^{-4}$. (b) The cubic friction force $F_c(v)$, where $b = 0.5$, $a = 1$ and $\alpha = 0.2$. (c) The piecewise linear friction force $F_0(v)$.
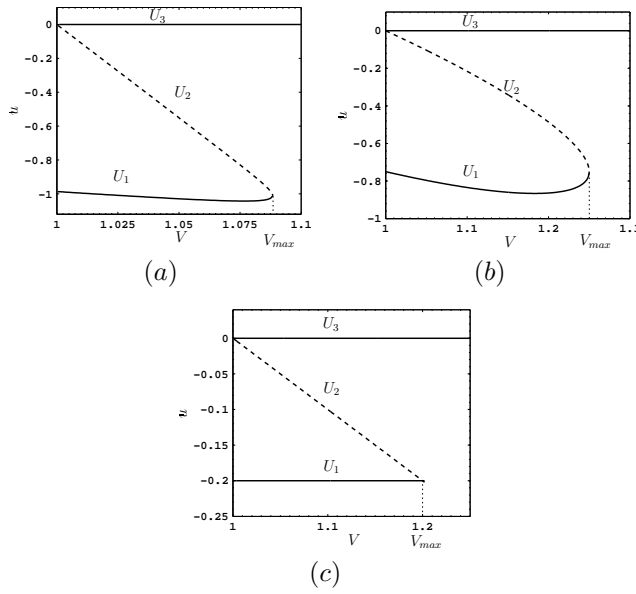
Figure 3: Bifurcation diagrams of the single block model. Stationary state, u, as a function of the stationary sliding velocity, V, for (a) regularized generalized Coulomb friction force F_ε ($a = 1$, $\alpha = 0.2$, $\varepsilon = 10^{-4}$) (b) the cubic friction force F_c and (c) the piecewise linear friction force F_0 ($a = 1$, $\alpha = 0.2$)). Solid lines represent stable states (denoted U_1 and U_3) and dotted lines are for unstable states (U_2).

The y-nullcline is defined by $u = 0$ whereas the u-nullcline is obtained by solving $F(V + u) = F(V)$ so that the vertical axis $u = 0$ always defines in the (u, y) plane the set of fixed points for an isolated block. It is easy to check that the two associated eigenvalues are given by $\lambda_1 = \frac{-F'(V)}{m}$, $\lambda_2 = 0$ so that the equilibrium straight line is stable (but not asymptotically stable). In (4), the dynamics of the velocity u does not depend on the position y so that system (4) behaves as a one dimensional dynamical system whose bifurcation diagram is shown in Fig. 3 for the three friction laws (3) where V is taken as the bifurcation parameter. For $V \in (a, V_{\max})$, where $V_{\max}$ is the velocity value such that $F(V_{\max})$ equals the local maximum in F and $V_{\max} > a$, there exist three fixed points $U_1 < U_2 < U_3 = 0$ whose stability is governed by the eigenvalue $\mu_i = \frac{-F'(V + U_i)}{m}$, $i \in \{1, 2, 3\}$, respectively. A saddle-node bifurcation occurs at $V = V_{\max}$ and a

transcritical bifurcation takes place at $V = a$. For $V \in (a, V_{\max})$, the two fixed points U_1 and U_3 are stable whereas U_2 is unstable and behaves as an excitation threshold. For an initial condition below U_2 the trajectory of the system tends towards $U_3 = 0$, whereas for a sufficiently strong perturbation the system reaches asymptotically the state U_1 illustrating the excitable dynamics of an isolated block. Depending on the initial state, the system can switch from a neighbourhood of U_3 to U_1 and vice versa. For the cubic friction force $F_c(v)$, the threshold is given by

$$U_2 = -\frac{3}{2}V + \frac{9}{8} + \frac{1}{8}\Delta(V) \tag{5}$$

where $\Delta(V) = \left(-48V^2 + 72V - 15\right)^{1/2}$ (one has $\Delta(V) \in \mathbb{R}$ for $V \in [1/4, 5/4]$). We have

$$U_1 = -\frac{3}{2}V + \frac{9}{8} - \frac{1}{8}\Delta(V),$$

and $V_{\max} = 5/4$. For the friction force $F_0(v)$, the threshold is simply defined as

$$U_2 = a - V, \tag{6}$$

the stable fixed point u_1 is given by

$$U_1 = -\alpha a, \tag{7}$$

and we have $V_{\max} = a(1 + \alpha)$. For the regularized generalized Coulomb law F_ε, as $\varepsilon \to 0$ the threshold converges to

$$U_2 = (a - V)\left[1 + \frac{2}{\alpha}\right]$$

and the stable fixed point u_1 to

$$U_1 = -V$$

and we have $V_{\max} = a(1 + \frac{\alpha}{2})$. In the following we are interested in the excitability regime where the velocity of the single block has two stable steady states and we fix a V value in the interval delimited by the two bifurcation points, i.e. $V \in]a, V_{\max}[$. As we will show in the sequel, the bistability property is a key feature for the existence of travelling fronts in the block-spring chain.

4   Travelling waves

Let us consider the block-spring slider model with the regularized generalized Coulomb law F_ε. We choose parameters so that each block exhibits a bistable behaviour. The parameters of the friction law are those of Fig. 3(a). Model (2) can be rewritten in terms of velocity as

$$m\frac{d^2 u_n}{dt^2} \;\; = \;\; k\Delta_d u_n - \frac{du_n}{dt}F'(V + u_n). \tag{8}$$

We initialize the network by applying a suitable perturbation to the steady state $U_3 = 0$. A localized perturbation is applied on the first block at the left edge of the network, see Fig. 4 for more details. We consider a finite chain of blocks with free boundary conditions. For the numerical simulations, we use the adaptive Lsoda solver with a time step $\Delta t = 0.001$ and with a minimal error tolerance of $1.5e - 8$. Unless stated otherwise, we take $m = 0.15$. We observe the existence of travelling fronts as shown in Fig. 4(a). In addition, two types of pulse solutions
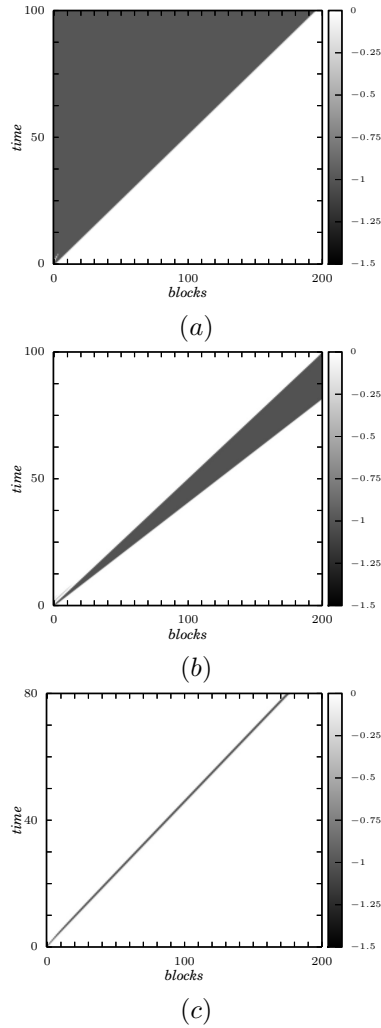
Figure 4: Numerical simulations of equation (8) with the regularized Coulomb friction force F_ε with the same parameters as in Fig. 3. We display spatiotemporal plots of the velocity variable u_n of (a) a travelling front ($k = 0.5$ and $V = 1.01$), (b) a broadening pulse ($k = 1$ and $V = 1.025$), (c) a steadily propagating pulse solution ($k = 1$ and $V = 1.046$). An initial perturbation $u_0(0) = -10$ is applied on the first block of the chain. Computations are performed for $m = 0.15$.

are observed: (i) pulse waves with expanding width and (ii) pulse waves with constant shape as plotted in Fig. 4(b) and (c), respectively. Propagating fronts (similar to the one shown in Fig. 4(a)) are the dominant pattern when the threshold is close to the resting state, i.e., for V close to a ($|U_2| \ll 1$). The speed of the propagating front increases with the coupling value k but, at the same time, the parameter range where front waves exist shrinks (without vanishing). As the stationary sliding velocity increases, a front to pulse transition occurs where the excitation spreads over the network and leads to pulses with expanding width (see Fig. 4(b)). The rate of expansion of the enlarging pulse decreases as the sliding velocity increases leading to the existence
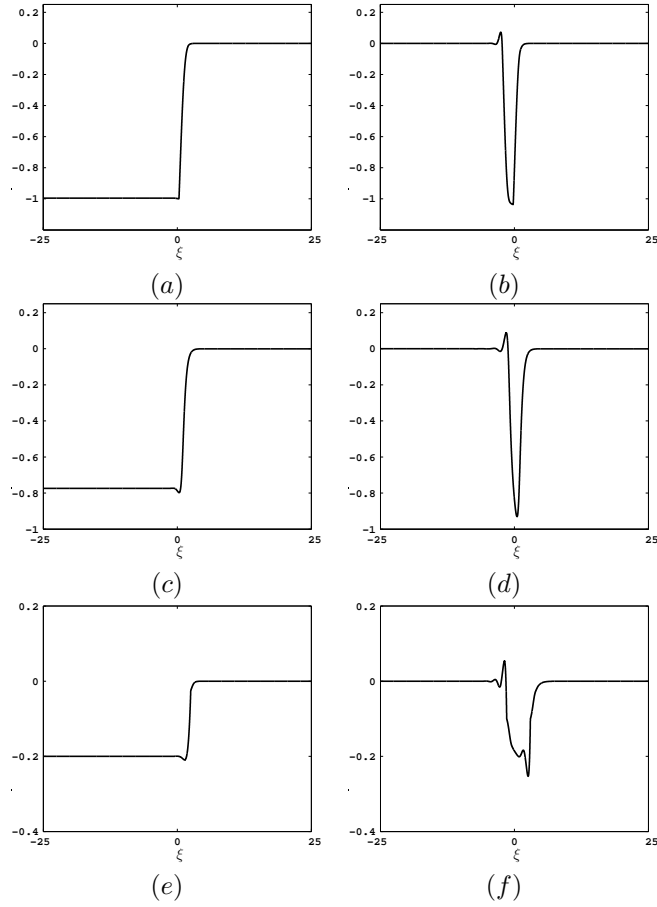
Figure 5: Plots of the velocity waveforms $u_n(t)$ of the block-spring model in the travelling wave coordinate $\xi = n - ct$. The wave profiles in (a,b) are obtained with the regularized generalized Coulomb law F_ε and correspond to the travelling waves shown in Fig. 4(a,c), respectively. Plots (c) and (d) represent the wave profiles obtained with the cubic friction force, F_c. Plots (e) and (f) represent the wave profiles obtained with the piecewise linear friction law F_0. The wave speed is (a) $c = 1.95$, (b) $c = 2.21$, (c) $c = 3.06$, (d) $c = 3.16$, (e) $c = 3.16$ (f) $c = 1.45$. For the piecewise linear law, we use $a = 1$ and $\alpha = 0.2$. Other parameters are those of Fig. 4 for (a-b) and we take (c) $V = 1.025$, $k = 1$ (d) $V = 1.18$, $k = 2$, (e), $V = 1.025$, $k = 1$, (f) $V = 1.1$, $k = 1$.

of a pulse with constant width as shown in Fig. 4(c). For $V \to V_{\max}$, the threshold approaches the fixed point U_1 and a perturbation fails to produce a travelling pattern. Qualitatively similar results are obtained for the cubic friction force F_c and for the piecewise linear friction force F_0. The profiles of the travelling waves observed in Fig. 4(a,c) are shown in Fig. 5(a,b), respectively, and are compared with those obtained with the cubic law (Fig. 5(c,d)) and the piecewise-linear law (Fig. 5(e,f)). The travelling patterns for the three friction forces have similar shapes and mainly contrast in their amplitude that is determined by the distance between the two stable fixed points. A non-monotonic wave profile is observed for the travelling fronts with the existence of a dip behind the front (see Fig.5(c, e) whereas the dip is too small to be seen in Fig.5(a)). Interestingly, similar profiles were obtained for traveling fronts in a chain of bistable oscillators

[7]. Qualitatively, these results are not affected by the mass parameter (simulations not shown). The enlarging pulse observed in Fig. 4(b) may be seen as the superposition of two travelling fronts with two different propagating speeds (see Fig. 6). The initial front is qualitatively similar to the waveform shown in Fig. 5(a) and is followed by a travelling front that propagates in the same direction but with a lower speed and that connects the two stable states in a reversed order. The localized pulse waves shown in Fig. 5(b,d,f) are thus expected to appear when the two travelling fronts have the same speed. These observations are analytically explained in the next section for the piecewise-linear law F_0.
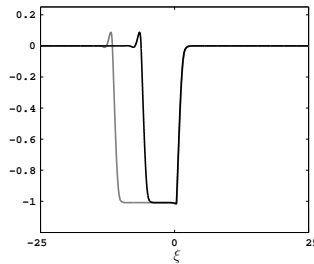
Figure 6: Plot of the velocity waveforms $u_n(t)$ of the block-spring model. The two localized pulses correspond to a snapshot of the travelling pattern shown in Fig. 4(b) at two different locations ($n = 25$, $n = 50$). The initial front propagates at speed $c = 2.45$ and the rear front at $c = 2$. Other parameters are those of Fig. 4(b)

5   Construction of travelling fronts for the piecewise-linear friction force

A travelling front solution of (8) takes the form:

$$u_n(t) = \varphi(n - c\,t) \tag{9}$$

where

$$\varphi(\infty) = U_3 = 0 \quad \text{and} \quad \varphi(-\infty) = U_1 \tag{10}$$

with $U_1 \neq 0$ a stable equilibrium. The function φ describes the waveform, and c is the wave speed that has to be determined. Substitution of (9) into (8) gives the advance-delay differential equation

$$c^2 m \varphi''(\xi) = k(\varphi(\xi + 1) + \varphi(\xi - 1) - 2\varphi(\xi)) + c\frac{d}{d\xi}F_0(V + \varphi(\xi)) \tag{11}$$

where $\xi = n - ct \in \mathbb{R}$ is the travelling wave coordinate. Front solutions connect two different stable steady states as $n \to \pm\infty$. In contrast, travelling pulses tend towards the same stable equilibrium as $n \to \pm\infty$.

We consider here the piecewise linear force F_0 and we assume that each block is in a bistable regime, i.e. we have $V \in (a, a(1 + \alpha))$ and $U_1 = -\alpha a$ as in (7). We assume that the travelling front solution crosses the threshold (6) for only one value of ξ. Translation invariance of travelling waves allows us to fix this value to $\xi = 0$ and we seek for a solution such that

$$\begin{cases} \varphi(\xi) < a - V \text{ for } \xi < 0, \\ \varphi(0) = a - V, \\ \varphi(\xi) > a - V \text{ for } \xi > 0. \end{cases} \tag{12}$$

Using (12) to simplify the nonlinear term $F_0(V + \varphi)$, system (11) takes the form

$$
\begin{aligned}
c^2 m \varphi''(\xi) \quad &= \quad k\left[\varphi(\xi+1) + \varphi(\xi-1) - 2\varphi(\xi)\right] + \dots \\
&\quad \frac{c}{a}\varphi'(\xi) - \alpha c\delta(\xi),
\end{aligned}
\tag{13}
$$

where $\delta(\xi)$ is the Dirac delta function.

Equation (13) is a linear non-autonomous differential equation so that one may attempt to use the Fourier transform to derive an analytic solution. However a certain amount of care is needed to correctly handle the Fourier transform of φ due to the nonzero boundary condition at $-\infty$. We look for $\varphi(\xi)$ in the form

$$
\begin{cases}
\varphi(\xi) = \alpha a\left[\psi(\xi) + H(\xi) - 1\right], \\
\psi(\xi) \in L^2(\mathbb{R}), \quad \lim_{\xi \to \pm\infty} \psi(\xi) = 0,
\end{cases}
\tag{14}
$$

where $\psi(\xi)$ has to be determined. Equation (13) is re-expressed in terms of $\psi(\xi)$ and Fourier transform is applied to determine $\psi(\xi)$, and subsequently $\varphi(\xi)$.

Integrating (13), gives

$$
c^2 m \varphi' \quad = \quad k \wedge' * \varphi + \frac{c}{a}\varphi + \alpha c(1 - H),
\tag{15}
$$

where $\wedge(\xi) = \max\left(1 - |\xi|, 0\right)$ is the tent function, and where we used for any $f \in L^1_{loc}(\mathbb{R})$,

$$
(\wedge' * f)(\xi) = \int_{\xi}^{\xi+1} f(s)ds - \int_{\xi-1}^{\xi} f(s)ds.
\tag{16}
$$

Note that (15) together with (10) remains equivalent to the original problem (13)-(10). Injecting (14) into (15), gives

$$
c^2 m \psi' - \frac{c}{a}\psi - k \wedge' * \psi \quad = \quad k \wedge - c^2 m\delta,
\tag{17}
$$

where we used the property $\wedge' * (H - 1) = \wedge$. Taking the Fourier transform as $\widehat{\psi}(\lambda) = \int_{\mathbb{R}} e^{-2\pi i\lambda\xi}\psi(\xi)d\xi$ in (17), we obtain

$$
\left[2i\pi\lambda c^2 m - \frac{c}{a} - k2i\pi\lambda\mathrm{sinc}^2(\lambda)\right]\widehat{\psi}(\lambda) = k\mathrm{sinc}^2(\lambda) - c^2 m,
\tag{18}
$$

where we used $\widehat{\wedge}(\lambda) = \mathrm{sinc}^2(\lambda)$ with $\mathrm{sinc}(\lambda) = \sin(\pi\lambda)/\pi\lambda$. Let us introduce

$$
\widehat{K}(\lambda) = \left(2i\pi\lambda\left[c^2 m - k\mathrm{sinc}^2(\lambda)\right] - \frac{c}{a}\right)^{-1}
$$

where one has $\widehat{K}(\lambda), K(\xi) \in L^2(\mathbb{R})$ (K denotes the inverse Fourier transform of $\hat{K}$). From $\frac{d\widehat{K}}{d\lambda} \in L^1(\mathbb{R})$ and using $-2i\pi\xi K = \mathcal{F}^{-1}\left(\frac{d\widehat{K}}{d\lambda}\right) \in L^{\infty}(\mathbb{R})$, one has $\lim_{\xi \to \pm\infty} K(\xi) = 0$ ($\mathcal{F}^{-1}$ denotes the inverse Fourier transform). From (18), we obtain

$$
\psi = kK * \wedge - c^2 mK.
\tag{19}
$$

Since $\wedge \in L^1(\mathbb{R})$ we have $K * \wedge \in L^2(\mathbb{R})$, and because $K, \wedge \in L^2(\mathbb{R})$ then $K * \wedge \in C^0(\mathbb{R})$ decays to zero when $\xi \to \pm\infty$. Consequently $\psi(\xi)$ given by (19) satisfies the properties assumed in (14), and defines a unique solution in $L^2(\mathbb{R})$. Therefore (14) is a solution of (13) with boundary

conditions (10). Regularity properties of $\varphi(\xi)$ can be inferred from the following identity obtained from (14) and (17)

$$\frac{c^2 m}{\alpha a}\varphi' = \frac{c}{a}\psi + k \wedge' * \psi + k \wedge . \tag{20}$$

This implies $\varphi' \in L^1_{loc}(\mathbb{R})$ (since $\wedge' * \psi \in L^2(\mathbb{R})$) and thus ones has $\varphi \in C^0(\mathbb{R})$. We also get from (15) that $\varphi' \in C^0(\mathbb{R}^+) \cap C^0(\mathbb{R}^-)$, hence $\varphi \in C^1(\mathbb{R}^+) \cap C^1(\mathbb{R}^-)$, and thus (15) gives $\varphi' \in C^1(\mathbb{R}^+) \cap C^1(\mathbb{R}^-)$. We get finally

$$\varphi \in C^2(\mathbb{R}^+) \cap C^2(\mathbb{R}^-) \cap C^0(\mathbb{R}).$$

From the analytical expression of φ, we can derive an equation to determine the wave speed of the front. Using (14), we set

$$\frac{\varphi(\xi) + \varphi(-\xi)}{2} = \frac{\alpha a}{2}[\psi(\xi) + \psi(-\xi) - 1] \tag{21}$$

where ψ is defined by (19) (note that we used $H(-\xi) = 1 - H(\xi)$ to eliminate the Heaviside function). Using the threshold condition $\varphi(0) = a - V$ from (12) together with (21) and (19), we obtain that the wave speed satisfies

$$\alpha a c^2 m[K(0^+) + K(0^-)] + 2(a - V) + 1 = 0. \tag{22}$$

This scalar equation allows us to compute c numerically using a Newton-type method. Computation of K is done using a Gauss-Konrod quadrature formula in a truncated interval $[-10^6, 10^6]$. We restrict to $c > 0$ (the case $c < 0$ can be deduced by symmetry, see section 7). A plot of the resulting analytical profile (14) is shown in Fig. 7(a) and compared with the numerical simulation of (8). A perfect matching is realized between the two trajectories. The typical dependence of the wave speed on the stationary sliding velocity, V, and on the coupling, k, is shown in Fig. 7(b).

6   Anti-continuum limit

In this section the small coupling limit is explored. We consider the case $c > 0$ (see section 7 for the case $c < 0$). From (17) and (19) with $k \to 0$, we have the leading order equation

$$c^2 m K' - \frac{c}{a}K - k \wedge' * K = \delta, \tag{23}$$

where we look for a solution of the form

$$K = K_0 + kK_1 + \mathcal{O}(k^2). \tag{24}$$

Inserting (24) in (23), and equating orders of leading terms in k, we obtain

$$c^2 m(K_0' - \nu K_0) = \delta, \tag{25}$$
$$c^2 m(K_1' - \nu K_1) = \wedge' * K_0, \tag{26}$$

where $\nu^{-1} = cam$. Observe (25) has the unique bounded solution

$$K_0(\xi) = -\frac{1}{c^2 m}e^{\nu\xi}H(-\xi), \tag{27}$$
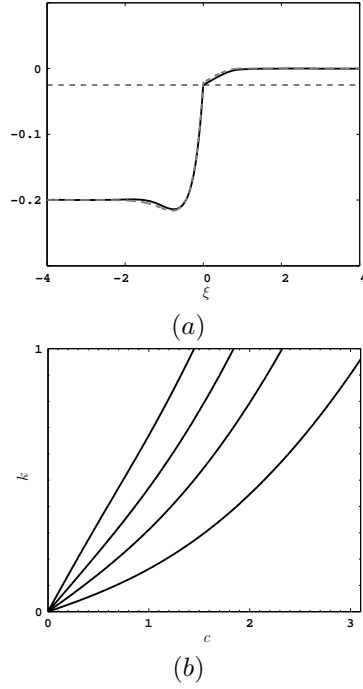
Figure 7: (a) Travelling front solution computed from the explicit formula (14) where $k = 0.3$, $V = 1.025$, $a = 1$ and $\alpha = 0.2$ (full line). The trajectory is indistinguishable from the ones obtained from the numerical simulation of the chain. The asymptotic approximation (29) obtained for $k \ll 1$ is also shown (dashed grey). We obtain $c = 1.55$ from the threshold condition (12) (the dashed line defines the threshold $u_2 = a - V$). (b) Wave speed curves in the (c, k) plane obtained from (22) for $V = 1.025$, 1.05, 1.075 and 1.1 (from right to left, respectively).

where $K_0 \in L^1(\mathbb{R})$, hence the solution of (26) reads

$$
\begin{aligned}
K_1 &= K_0 * \wedge' * K_0 = \wedge * K_0 * K_0', \\
&= \frac{1}{c^2 m} \wedge * K_0 + \nu \wedge * K_0 * K_0,
\end{aligned}
\tag{28}
$$

where we used $K_0' = \frac{1}{c^2 m}\delta + \nu K_0$. Using (19) with (27) and (28), the approximation for φ up to $\mathcal{O}(k^2)$ reads

$$
\begin{aligned}
\varphi(\xi) &= \alpha a(e^{\nu\xi} - 1)H(-\xi) + \alpha a k \big[-c^2 m K_1(\xi) + \ldots \\
&\quad (K_0 * \wedge)(\xi) \big] + \mathcal{O}(k^2)
\end{aligned}
\tag{29}
$$

where we used the identity $H(-\xi) = 1 - H(\xi)$.

Expression (29) allows to obtain an approximation of the wave speed c for small k. From $\varphi(0) = a - V$ and (29), we get

$$
\begin{aligned}
a - V &= \alpha a k \left(-c^2 m K_1(0) + (K_0 * \wedge)(0)\right) + \mathcal{O}(k^2), \\
&= -\alpha k c (\wedge * K_0 * K_0)(0) + \mathcal{O}(k^2), \\
&:= S(c)k + \mathcal{O}(k^2).
\end{aligned}
\tag{30}
$$

(a)

(b)
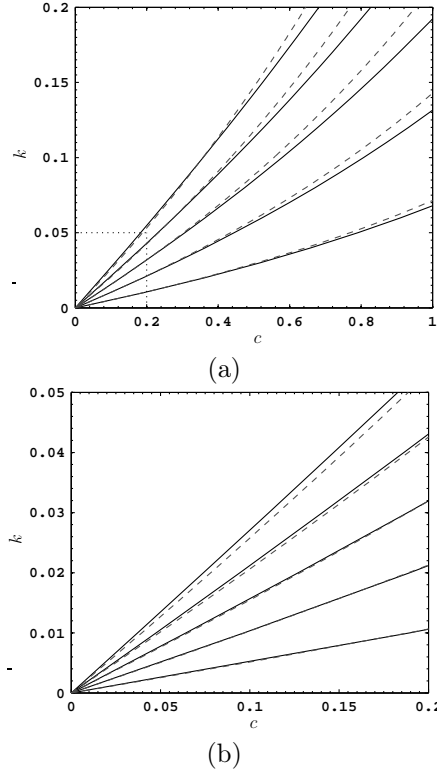
Figure 8: (a) Speed curves of the travelling front solution in the (c, k) plane for $V = 1.0025, 1.005, 1.0075$ and 1.01 (from right to left, respectively). Curve solutions (c, k) computed with (34) (dashed grey) accurately describes the exact curves (c, k) computed with (22) (black continuous) in the limit $c \to 0$. (b) A zoom of the dashed square region in panel (a) is shown. Parameter values are $\alpha = 0.2$ and $a = 1$.

We obtain after some calculations (see appendix A)

$$S(c) = 2\alpha m a^3 - \frac{\alpha a^2}{c}\left((2amc + 1)e^{-1/amc} + 1\right) \tag{31}$$

In order to approximate c, we drop $\mathcal{O}(k^2)$ terms in (30). The wave speed can be estimated from the solution of

$$\nu - 2 + (\nu + 2)e^{-\nu} = \frac{V - a}{\alpha m a^3 k} \tag{32}$$

where $\nu^{-1} = acm$. It can be shown that the left-hand side of (32) defines a bijective function on $\mathbb{R}$ that passes through the origin so that (32) admits a unique solution. Let fix the values of V and a, and look for solutions $c \approx 0$ when $k \approx 0$. Observing the exponential decay $e^{-\nu} \to 0$ as $c \to 0$, we have, from (31) and (30) the leading order approximation

$$\nu = 2 + \frac{V - a}{\alpha m a^3 k} \tag{33}$$

for $k, c \to 0$. Therefore we obtain the following approximation for the wave speed

$$c \sim \frac{1}{2am + \frac{V-a}{\alpha a^2 k}} \tag{34}$$

where the leading order approximation reads $c \sim \frac{\alpha a^2 k}{V-a}$.

Formula (34) was derived under the assumption that c is small for k small, and one can easily check that c given by (34) satisfies $c \to 0$ as $k \to 0$. To evaluate the accuracy of the asymptotic approximation (34), we compare in Fig. 8 the (c, k) curves obtained from (22) with those computed from (34) for different sliding velocities V. The asymptotic approximation (29) of the waveform is compared with the exact solution (see Fig. 7(a)). A good matching between the two wave profiles is found. Monotonicity analysis of the approximated waveform (29) shows that the velocity profile is nonmonotonic, i.e. a dip always exists behind the front (see appendix B).

7   Reverse travelling fronts and pulses

In the previous section we have constructed travelling fronts connecting the two stable equilibria $U_1 = -\alpha a$ (when $n \to -\infty$) and 0 (when $n \to +\infty$). In this analysis we have restricted our attention to travelling fronts with positive velocity $c(V)$ (for now we consider the dependency of front velocity in V and discard the other parameters). Using symmetry arguments, we show in the sequel the existence of travelling fronts with negative velocity *satisfying the same boundary conditions*. We also deduce the existence of travelling fronts with positive velocity satisfying reverse boundary conditions ($u_n \to -\alpha a$ when $n \to +\infty$ and $u_n \to 0$ when $n \to +\infty$).

Let us start with some symmetry considerations. Consider the advance-delay equation (11) with boundary conditions

$$\varphi(-\infty) = U_1, \qquad \varphi(+\infty) = U_3. \tag{35}$$

This problem admits the invariance

$$\varphi(\xi) \to \varphi(-\xi), \quad c \to -c, \quad (U_1, U_3) \to (U_3, U_1). \tag{36}$$

Moreover, the piecewise-linear friction force F_0 is antisymmetric about $v = a$, i.e. we have

$$F_0(a + h) + F_0(a - h) = 2 - \alpha, \quad \text{for all } h \in \mathbb{R}.$$

As a consequence, one can readily check that (11)-(35) is invariant by the one-parameter family of transformations

$$\varphi \to -\lambda - \varphi, \quad V \to 2\,a + \lambda - V, \quad (U_1, U_3) \to (-\lambda - U_1, -\lambda - U_3), \tag{37}$$

where $\lambda \in \mathbb{R}$ is arbitrary.

Now let us use the above invariances in order to obtain reverse travelling fronts. We define $\tilde{\zeta} = -\alpha\,a - \varphi$, so that $\tilde{\zeta}$ and φ connect stable equilibria in reverse order at infinity. Applying invariance (37) for $U_3 = 0$ and $\lambda = \alpha\,a = -U_1$, it follows that φ is a solution of (11) if and only if $\tilde{\zeta}$ is a solution of the same equation with modified sliding velocity $\tilde{V} = a(2 + \alpha) - V$. From the results of section 5, this problem admits for all $\tilde{V} \in (a, a(1 + \alpha))$ a front solution $\tilde{\zeta}$ satisfying the boundary conditions $\tilde{\zeta}(-\infty) = -\alpha a$, $\tilde{\zeta}(+\infty) = 0$, with velocity $c(\tilde{V}) > 0$. From invariance (36), this equation possesses another front solution $\zeta(\xi) = \tilde{\zeta}(-\xi)$ with velocity $-c(\tilde{V}) < 0$, which satisfies the boundary conditions $\zeta(+\infty) = -\alpha a$, $\zeta(-\infty) = 0$. It follows that for all $V \in (a, a(1 + \alpha))$, equation (11) with sliding velocity V admits the front solution $\tilde{\varphi} = -\alpha\,a - \zeta$, satisfying the boundary conditions (10) and having a negative velocity $-c(a\,(2+\alpha)-V)$. Consequently, the search of front solutions of (10)-(11) can be reduced to the case $c > 0$ examined in section 5, since all fronts with $c < 0$ can be deduced by symmetry.

Furthermore, $\varphi(\xi) = \tilde{\varphi}(-\xi) = -\alpha\,a - \tilde{\zeta}(\xi)$ defines another solution of (11) with sliding velocity V. This front has a positive velocity $c(\tilde{V}) = c(a\,(2+\alpha) - V)$ and satisfies the reverse boundary conditions

$$\varphi(-\infty) = 0, \qquad \varphi(+\infty) = -\alpha a. \tag{38}$$

The coexistence of this reverse front and the front satisfying (10)-(11) with the different velocity $c(V)$ can be used to understand the broadening of pulses reported in section **??**, as well as the existence of steadily propagating pulses observed for particular sliding velocities. Indeed, we can see from Fig. 8(b) that the function $V \mapsto c(V)$ is decreasing (this is also clear from the leading order approximation (34)). Consequently, gluing the two above fronts to form a pulse decaying to 0 at infinity, the trailing front (at the rear of the propagating pulse) will be slower if $V < \tilde{V}$, resulting in a broadening of the pulse. This regime occurs for $V \in (a, a(1 + \frac{\alpha}{2}))$. In the critical case $V = a(1 + \frac{\alpha}{2})$, we have $V = \tilde{V}$ and the two fronts have identical velocities, thereby maintaining a steadily propagating pulse (this case is shown in Fig. 5(f)). Conversely, for $V \in (a(1 + \frac{\alpha}{2}), a(1 + \alpha))$, the trailing front is faster and no pulse wave can propagate. Starting from an initial bump condition, an annihilation occurs when the trailing front reaches the leading front. In conclusion, the condition for the existence of broadening pulses reads

$$V < V^* \quad \text{where} \quad V^* = a\left(\frac{\alpha}{2} + 1\right). \tag{39}$$

For $V > V^*$, pulse fails to propagate whereas for $V = V^*$ a stable pulse is observed, with a width determined by the initial perturbation. In the small coupling limit, this pulse has a wave speed $c \sim 2ak$ according to approximation (34).

8 Discussion

We studied localized travelling waves in a nonlinear lattice describing a block-spring chain sliding down a slope and experiencing friction. Wave propagation was illustrated for different spinodal friction laws. For a particular range of stationary sliding velocities, the medium is made of blocks exhibiting bistabilities and supports nonlinear solitary transition waves (wave fronts). Interesting links can be made with recent results on waves in bistable lattices [17, 16]. For an idealized piecewise-linear friction force, we constructed analytically travelling fronts and analysed their wave speeds. In contrast with the discrete Nagumo equation, propagating fronts exist at small coupling values, i.e., propagation failure does not occur atnweak coupling strength. As already observed in a different context [22], the travelling pulses are shaped by the concatenation of two travelling front solutions and pulse propagation failure occurs when the back wave is faster than the front wave. We determined analytically the parameter range where pulses of constant width occur, i.e., the leading front and the trailing front have the same velocity. It is worth noting that this analysis does not rely on a time scale separation and differs from the asymptotic construction of pulses done in [4]. In particular, the pulse width is not determined by the equality of the velocity of the two fronts but depends on the initial excitation.

The present study is also of interest for the understanding of the dynamics of the Burridge-Knopoff model where the time evolution of the system is given by

$$\gamma \ddot{y}_n = k_c \Delta_d y_n - F(V + \dot{y}_n) - y_n. \tag{40}$$

Let us define $y_n(t) = -F(V) + \gamma z_n(t/\gamma)$ and $k = \gamma k_c$. Assuming $\gamma \ll 1$, then, the Burridge-Knopoff model (40) can be rewritten in the fast time scale as

$$\ddot{z}_n = k \Delta_d z_n - F(V + \dot{z}_n) + F(V)$$

that coincides with (2). Therefore, for small γ values, the front waves of (2) provide useful information on the dynamics of pulse propagation in the Burridge-Knopoff model (40). More precisely, fronts approximate the transition region from the ground state to the excited state. This is shown in Fig. 9 where the fast time scale of the Burridge-Knopoff model is accurately reproduced by model (2).
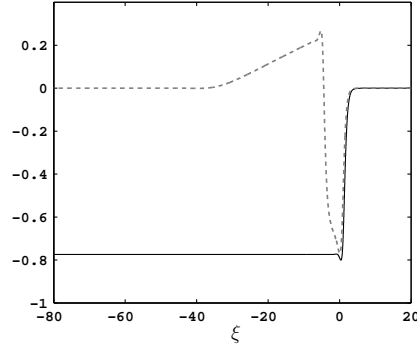
Figure 9: Comparison of a front solution of (2) (solid line) with a pulse supported by the Burridge-Knopoff model (dotted line). Computations are performed for the cubic friction law F_c and the following parameters : $\gamma = 0.05$, $k_c = 10$, $V = 1.025$.

A   Computation of $S(c)$

We compute here the explicit expression of $S(c) = -\alpha c \left(\wedge * K_0 * K_0 \right)(0)$. We reexpress K_0 as $K_0(\xi) = -\frac{G(\xi)}{c^2 m}$ where $G(\xi) = e^\nu H(-\xi)$, hence we have

$$S(c) = -\frac{\alpha}{c^3 m^2} \left(\wedge * G * G \right)(0). \tag{41}$$

We have

$$(G * G)(-s) = \int_{-s}^{0} G(\tau) G(-s-\tau) d\tau = s e^{-\nu s} H(s)$$

with $s > 0$, therefore

$$
\begin{aligned}
\left(\wedge * G * G \right)(0) &= \int_{\mathbb{R}} \wedge(\tau)(G * G)(-\tau) d\tau \\
&= \int_0^1 (1-\tau)(\tau e^{-\nu\tau}) d\tau \\
&= \frac{\nu + e^{-\nu}\nu - 2 + 2e^{-\nu}}{\nu^3} \\
&= \frac{e^{-\nu}}{\nu^3}(2+\nu) + \frac{-2+\nu}{\nu^3}
\end{aligned}
$$

with $\nu = (cam)^{-1}$. We further calculate

$$\frac{e^{-\nu}}{\nu^3}(2+\nu) + \frac{-2+\nu}{\nu^3} = -\nu^{-2} \left[2\nu^{-1} - (2\nu^{-1}+1)e^{-\nu} - 1 \right] \tag{42}$$

Inserting (42) into (41), gives

$$S(c) = \frac{\alpha \nu^{-2}}{c^3 m^2} \left[2\nu^{-1} - 1 - (2\nu^{-1}+1)e^{-\nu} \right], \tag{43}$$

and (31) follows.

B   Monotonicity of the approximated front

From (28) and (29) one has the following asymptotic approximation of the wavefrom

$$\varphi(\xi) \quad = \quad \alpha a(e^{\nu\xi}-1)H(-\xi) - \alpha ck \wedge *K_0 * K_0(\xi) + \mathcal{O}(k^2)$$

We note $\varphi_1 = \wedge * K_0 * K_0$ and we calculate $\varphi_1 = 0$ for $\xi \geq 1$ and

$$\varphi_1(\xi) \quad = \quad \frac{1}{m^2c^4\nu^3}\big((2+\nu(1-\xi)e^{\nu(\xi-1)} + \dots \\ +(2-\nu(1+\xi)e^{\nu(\xi+1)} + (2\nu\xi-4)e^{\nu\xi}\big)$$

for $\xi \leq -1$. For $\xi \ll 0$ we obtain the following approximation

$$\varphi_1(\xi) \quad \sim \quad -\frac{2(\cosh(\nu)-1)}{m^2c^4\nu^2}\xi e^{\nu\xi}.$$

Therefore the travelling front takes the leading form

$$\varphi(\xi) \quad \sim \quad -\alpha a + \frac{2\alpha(\cosh(\nu)-1)k}{m^2c^3\nu^2}\xi e^{\nu\xi}$$

as $\xi \ll 0$. Using $c \sim \frac{\alpha a^2 k}{V-a}$ we have

$$\varphi(\xi) \quad \sim \quad -\alpha a + 2(V-a)(\cosh(\nu)-1)\xi e^{\nu\xi} \tag{44}$$

that is a decreasing function of ξ for $\xi \ll 0$. The leading approximation of the wavefront is zero for $\xi \geq 1$ and has a decreasing profile for ξ sufficiently small, therefore the wavefront is nonmonotonic and presents (at least) one dip after the front. Notice that the function occuring on the righthand side of (44) has a minimum at $\xi = -1/\nu$ that may be used to approximate the dip location.

References

[1] W. Atkinson and N. Cabrera. Motion of a Frenkel-Kontorova dislocation in a one-dimensional crystal. *Phys. Rev. A*, 138:763â766, 1965.

[2] R. Burridge and L. Knopoff. Model and theoretical seismicity. *Bull. Seismol. Soc. Am.*, 57:341–371, 1967.

[3] J. W. Cahn, J. Mallet-Paret, and E. S. Van Vleck. Traveling wave solutions for systems of ODEs on a two-dimensional spatial lattice. *SIAM J. Appl. Math.*, 59:455–493, 1999.

[4] A. Carpio and L. Bonilla. Pulse propagation in discrete systems of coupled excitable cells. *SIAM J. Appl. Math.*, 63:619–635, 2002.

[5] J. H. E. Cartwright, V. M. Eguíluz, E. Hernández-García, and O. Piro. Dynamics of elastic excitable media. *Int J. Bif. Chaos*, 9:2197–2202, 1999.

[6] J. H. E. Cartwright, E. Hernández-García, and O. Piro. Burridge-Knopoff models as elastic excitable media. *Phys. Rev. Lett.*, 79:527–530, 1997.

[7] M. Duanmu, N. Whitaker, P. G. Kevrekidis, A. Vainchtein, and J. Rubin. Traveling wave solutions in a chain of periodically forced coupled nonlinear oscillators. *Physica D*, 325:026615, 2002.

[8] C. E. Elmer and E. S. Van Vleck. Spatially discrete FitzHugh-Nagumo equations. *SIAM J. Appl. Math.*, 65:1153–1174, 2005.

[9] G. Ermentrout and D. Terman. *Mathematical foundations of neuroscience.* Springer, 2010.

[10] N. Flytzanis, S. Crowley, and V. Celli. High velocity dislocation motion and interatomic force law. *J. Phys. Chem. Solids*, 38:539–552, 1976.

[11] E. M. Izhikevich. *Dynamical systems in neuroscience: The geometry of excitability and bursting.* The MIT Press, 2007.

[12] Y. S. Kivshar, F. Zhang, and S. Takeno. Nonlinear surface modes in monoatomic and diatomic lattices. *Phys. D: Nonlinear Phenomena*, 113:248–260, 1998.

[13] P. Maniadis and S. Flach. Mechanism of discrete breather excitation in driven micro-mechanical cantilever arrays. *Europhys. Lett.*, 74:452–458, 2006.

[14] C. B. Muratov. Traveling wave solutions in the Burridge-Knopoff model. *Phys. Rev. E*, 59:3847–3857, 1999.

[15] J. Murray. *Mathematical biology.* Biomathematics. Springer-Verlag Berlin Heidelberg, 1993.

[16] N. Nadkarni, A. Arrieta, C. Chong, D. Kochmann, and C. Daraio. Unidirectional transition waves in bistable lattices. *Phys. Rev. Lett.*, 116:244501, 2016.

[17] J. Raney, N. Nadkarni, C. Daraio, D. Kochmann, J. Lewis, and K. Bertoldi. Stable propagation of mechanical signals in soft media using stored elastic energy. *PNAS*, 113:9722–9727, 2016.

[18] J. Rhoads, S. W. Shaw, and K. L. Turner. Nonlinear dynamics and its applications in micro-and nanoresonators. *Proceedings of DSCC2008*, 158:1–30, 2008.

[19] P. Rosakis and A. Vainchtein. New solutions for slow moving kinks in a forced frenkel-kontorova chain. *Journal of Nonlinear Science*, 23:1089–1110, 2013.

[20] H. Schwetlick and J. Zimmer. Existence of dynamic phase transitions in a one-dimensional lattice model with piecewise quadratic interaction potential. *SIAM J. Math. Anal.*, 41:1231–1271, 2009.

[21] A. Tonnelier. McKean caricature of the FitzHugh-Nagumo model: traveling pulses in a discrete diffusive medium. *Phys. Rev. E*, 67:036105, 2003.

[22] A. Tonnelier. Stabilization of pulse waves through inhibition in a feedforward neural network. *PhysicaD*, 210:118, 2005.

[23] L. Truskinovsky and A. Vainchtein. Kinetics of martensitic phase transitions: Lattice model. *SIAM J. Appl. Math.*, 66:533–553, 2005.

[24] L. Truskinovsky and A. Vainchtein. Solitary waves in a nonintegrable fermi-pasta-ulam. *Physical Review E*, 90:42903, 2014.

[25] A. Vainchtein. The role of spinodal region in the kinetics of lattice phase transitions. *Journal of Mechanics and Physics of Solids*, 58:227–240, 2009.

Contents